Elsevier Editorial System(tm) for Journal of Power Sources
Manuscript Draft

Manuscript Number: POWER-D-11-02896R1

Title: Microstructure and performance of La0.58Sr0.4Co0.2Fe0.8O3-d cathodes deposited on BaCe0.2Zr0.7Y0.1O3-d by infiltration and spray pyrolysis

Article Type: Full Length Article

Keywords: BCZY, LSCF, PCFC, spray pyrolysis, cathode material, infiltration

Corresponding Author: Dr Sandrine Ricote,

Corresponding Author's Institution: Risø DTU

First Author: Sandrine Ricote

Order of Authors: Sandrine Ricote; Nikolaos Bonanos, Dr; Per Martin Rørvik, Dr; Camilla Haavik, Dr

Abstract: La0.58Sr0.4Co0.2Fe0.8O3-d (LSCF) cathodes have been deposited on proton-conducting BaCe0.2Zr0.7Y0.1O3-d (BCZY27) electrolyte and studied in symmetric cells to investigate the cathode microstructure and electro-chemical performance. Three different types of cathodes have been prepared: two prepared from a solution, infiltrated into a screen-printed BZCY27 porous backbone (4 and 12 infiltrations), and one prepared by spray pyrolysis onto a polished electrolyte. In all three cases, LSCF is obtained after annealing at 700°C for 2 h. Analysis of the electrochemical impedance spectra between 450°C and 600°C in air, with varying p(H2O), reveals that the charge transfer contribution is lowest for the backbone-infiltrated cathode while the oxygen dissociation/adsorption contribution is lowest for the spray-pyrolyzed cathode. The area specific resistances increase with the water vapour pressure. The area specific resistances obtained are 0.61 Ω*cm2 and 0.89 Ω*cm2 at 600°C for the spray-pyrolyzed LSCF cell in dry and humidified air, respectively; the corresponding resistances are 0.63 Ω*cm2 and 0.98 Ω*cm2 for the 12 times infiltrated LSCF cell. These resistances are the lowest reported for LSCF cathodes on Ba(Ce,Zr)O3-based electrolytes and show the promise of low-temperature fabrication methods for these systems.

Highlights

- Low-temperature solution routes for PCFC cathode fabrication are demonstrated
- The electrochemical properties are correlated to the cathodes' microstructure
- ASR for spray-pyrolyzed LSCF at 600ºC in air: 0.61 $\Omega \cdot cm^2$
- ASR for infiltrated LSCF at 600ºC in air: 0.63 $\Omega \cdot cm^2$

Microstructure and performance of $La_{0.58}Sr_{0.4}Co_{0.2}Fe_{0.8}O_{3-\delta}$ cathodes deposited on $BaCe_{0.2}Zr_{0.7}Y_{0.1}O_{3-\delta}$ by infiltration and spray pyrolysis

Sandrine Ricote [1], Nikolaos Bonanos [1], Per Martin Rørvik [2], Camilla Haavik [2]

[1] Department of Energy Conversion and Storage, Technical University of Denmark, Frederiksborgvej 399, DK-4000 Roskilde, Denmark

[2] SINTEF Materials and Chemistry, P.O. Box 124 Blindern, Oslo NO-0314, Norway

Abstract

$La_{0.58}Sr_{0.4}Co_{0.2}Fe_{0.8}O_{3-\delta}$ (LSCF) cathodes have been deposited on proton-conducting $BaCe_{0.2}Zr_{0.7}Y_{0.1}O_{3-\delta}$ (BCZY27) electrolyte and studied in symmetric cells to investigate the cathode microstructure and electro-chemical performance. Three different types of cathodes have been prepared: two prepared from a solution, infiltrated into a screen-printed BZCY27 porous backbone (4 and 12 infiltrations), and one prepared by spray pyrolysis onto a polished electrolyte. In all three cases, LSCF is obtained after annealing at 700°C for 2 h. Analysis of the electrochemical impedance spectra between 450°C and 600°C in air, with varying $p(H_2O)$, reveals that the charge transfer contribution is lowest for the backbone-infiltrated cathode while the oxygen dissociation/adsorption contribution is lowest for the spray-pyrolyzed cathode. The area specific resistances increase with the water vapour pressure. The area specific resistances obtained are 0.61 $\Omega \cdot cm^2$ and 0.89 $\Omega \cdot cm^2$ at 600°C for the spray-pyrolyzed LSCF cell in dry and humidified air, respectively; the corresponding resistances are 0.63 $\Omega \cdot cm^2$ and 0.98 $\Omega \cdot cm^2$ for the 12 times infiltrated LSCF cell. These resistances are the lowest reported for LSCF cathodes on $Ba(Ce,Zr)O_3$-based electrolytes and show the promise of low-temperature fabrication methods for these systems.

Keywords: BCZY, LSCF, PCFC, spray pyrolysis, cathode material, infiltration.

* Corresponding author: sari@dtu.dk

Department of Energy Conversion and Storage, Technical University of Denmark, Frederiksborgvej 399, DK-4000 Roskilde, Denmark

Phone: +45 46 77 56 41

Fax: + 45 46 77 58 58

1. Introduction

Protonic ceramic fuel cells (PCFCs) have received increased attention in recent years. PCFC have two main advantages compared to solid oxide fuel cells (SOFCs) with oxygen ion-conducting electrolytes: firstly, protons are smaller than oxygen ions and can migrate more easily through the electrolyte at intermediate operating temperatures (400-600°C); secondly, under operation water vapour is formed at the cathode, allowing a better utilization of the fuel and removal of the product. Several reviews have summarized the work made on high temperature proton conductors (HTPCs) [1-3]. For PCFCs, the anode materials are cermets based on the HTPC electrolyte material and nickel oxide [3]. More recently, many groups have been working on the development of cathode materials, as the cathode appears to be the main performance-limiting component when the operating temperature is lowered into the intermediate range. The most studied materials are mixed oxide ion and electron conductors with perovskite [4-16] or layered oxide structure [6,12,17-22], some of them being commonly used also for SOFCs: $Ba_{1-x}Sr_xFe_{1-y}Co_yO_{3-\delta}$ [4-6,12,20] and $La_{1-x}Sr_xFe_{1-y}Co_yO_{3-\delta}$ [6-8,12]. Since, in the PCFC, the water is formed at the cathode, the reaction sites are restricted to the electrolyte/cathode interface, if the cathode material is a mixed oxide ion and electron conductor without any considerable proton conductivity. To increase the active area where protons, electrons and oxygen gas can react, a mixed proton and electron conductor would be preferable, since the whole cathode surface would be active. However, no material has been found to have both high electronic and protonic conduction in wet oxidizing atmosphere (cathode atmosphere) [3]. Another option to increase the active area is to increase the number of triple phase boundaries, for instance by using a composite material made of a proton conductor and a mixed oxide ion and electron conductor. High power densities have been obtained with composite cathodes such as $Sm_{0.5}Sr_{0.5}CoO_{3-\delta}/BaZr_{0.1}Ce_{0.7}Y_{0.2}O_{3-\delta}$ [19] or $Ba_{0.5}Sr_{0.5}Co_{0.8}Fe_{0.2}O_{3-\delta}/BaZr_{0.1}Ce_{0.7}Y_{0.2}O_{3-\delta}$ [20]. Another advantage of using a composite cathode is to reduce thermal expansion coefficient mismatch with the electrolyte. However, Ba^{2+} inter-diffusion between the $BaCe_{0.9}Y_{0.1}O_{3-\delta}$ electrolyte and the $Ba_{0.5}Sr_{0.5}Co_{0.8}Fe_{0.2}O_{3-\delta}$ cathode was found for temperature above 1000°C [5]. This range of temperature is generally used to prepare composite cathodes. To avoid cation inter-diffusion

during the preparation of the cell, we have investigated the infiltration of a standard mixed oxide ion and electron conductor ($La_{0.58}Sr_{0.4}Co_{0.2}Fe_{0.8}O_{3-\delta}$, referred to as LSCF) into a porous backbone of a proton conductor ($BaCe_{0.2}Zr_{0.7}Y_{0.1}O_{3-\delta}$, referred to as BCZY27).

Infiltration has seen a recent interest in the field of SOFC for the preparation of composite electrodes, both anodes and cathodes. A solution containing the required cations is dropped onto or sucked into a porous backbone. The advantage of the technique is that the homogeneous mixing of the cations in the solution enables relatively low calcination temperatures, thus minimizing possible reactions and cation inter-diffusion. Furthermore, nano-sized particles are obtained, which have a large surface area and can improve surface–catalytic behavior. LSCF has been successfully infiltrated in porous Gd-doped ceria (GDC) [23]: 25 µm thick GDC porous backbones were infiltrated using a water-based nitrate solution followed by firing at 800°C for 2 h. The authors demonstrated the importance of the firing temperature of the backbones (a too low temperature will lead to poor contacts between the electrolyte and the backbone while a too high temperature will reduce the porosity of the backbone) and of the infiltrates (loss of the nano-size if the temperature is too high). LSCF has also been infiltrated in porous yttria-stabilized zirconia (YSZ) using water-based nitrate solutions [24-25], with firing temperatures down to 700°C. To get a uniform distribution of the infiltrate, the wetting properties are also important. Ethanol was found to be an effective additive to the water-based nitrate solution to lower its surface tension on the backbone [26]. In another study, the contact angle between GDC nitrate solution and zirconia- or ceria-based porous backbones was measured using different solvents, without any surfactant, and it was found that the droplet was fully spread when using ethanol as a solvent [27].

Other chemical solution deposition methods can also be used for cathode fabrication. Spray pyrolysis is a simple and cost-effective technique for film deposition onto a flat sample in reasonable time. A solution is fed to a nozzle where it is atomized by air pressure, ultrasonic waves, or a high electric field [28]. The spray is directed towards a heated substrate where the film is deposited. Usually the film will be amorphous and subsequent

annealing is necessary for crystallization. LSCF cathode films have been successfully deposited onto GDC electrolytes by both air blast [29] and electrostatic spray pyrolysis [30], with maximum processing temperatures as low as 650 °C [29]. Here we have used air blast spray pyrolysis to deposit highly porous LSCF films with a large surface area onto polished BZCY27 to compare with the backbone-infiltrated cathodes. Although the number of triple phase boundaries is lower for the spray-pyrolyzed cathode, due to the lack of backbone, the high surface area can reduce the polarization resistance related to oxygen dissociation and adsorption.

This study presents the comparison of the electrochemical properties of the two cathode types, obtained from impedance spectra of symmetric cells (cathode|proton-conducting electrolyte|cathode), and discusses the influence of the cathode microstructure on the performance.

2. Experimental

2.1. Preparation of the substrate

Dense BCZY27 electrolyte substrates were prepared by solid state reactive sintering. After drying, the precursors were weighed in stoichiometric proportions: $BaCO_3$ (Alfa Aesar, 99.95% (metal basis)), ZrO_2 (Tosoh TZ-0), CeO_2 (Aldrich, 99.9%, trace of metal basis, < 5 μm) and Y_2O_3 (Reacton, 99.99%). NiO (Alfa Aesar, 99% (metal basis)) was added as a sintering additive as 1 w% of synthesized compound. The first step in the preparation was a 24 h wet blending of the reactant powders in acetone containing PeOx binder (poly(2-ethyl-2-oxazoline), molar weight 5000 g/mol) and Kellox dispersant (fish oil) for obtaining a uniform homogeneous starting powder. After blending, the solutions were pan dried and the powders were screened to a 40 mesh screen and then to an 80 mesh screen. Bars (8 mm × 8 mm × 35 mm) or pellets (12 mm diameter) were made by uniaxial pressing and were sintered in air with the following heating schedule: heating to 450°C with a ramp of $60°C \cdot h^{-1}$, heating to 1500°C with a rate of $120°C \cdot h^{-1}$, dwell of 4 h and cooling with a ramp of $120°C \cdot h^{-1}$. The resulting black-coloured bars or pellets were cut in 700 μm thick slices. The surface of these substrates was polished by hand with a 500 SiC paper.

2.2. Preparation of the cathodes

The LSCF solution for both spray pyrolysis and infiltration was made by dissolving $La(NO_3)_3 \cdot 6H_2O$ (Merck, p.a., >96%), $SrCl_2 \cdot 6H_2O$ (Fluka, >99%), $Co(NO_3)_2 \cdot 6H_2O$ (Fluka, >98%) and $Fe(NO_3)_3 \cdot 9H_2O$ (Merck, >99%) in molar ratio La:Sr:Co:Fe = 0.58:0.4:0.2:0.8 in a 1:1 volume mixture of absolute ethanol (Arcus) and diethylene glycol butyl ether (Aldrich, >99.2%) to give a 0.04 M total salt concentration.

LSCF thin films were deposited onto polished BCZY27 substrates by air blast spray pyrolysis. The solution was pumped (Merck Hitachi L-7110 isocratic pump, 0.5 $mL \cdot min^{-1}$) to an airbrush (Badger no. 150) where it was atomized by 1 bar air pressure and sprayed onto a heated substrate with surface temperature 240±5 °C for 120 min. The distance between the airbrush nozzle and the substrate was 20.0 cm. For symmetric cells, the substrate was turned and the deposition was repeated after stabilization of the surface temperature. The samples were finally calcined at 700°C for 2 h in air (100°C·h^{-1}) to crystallize and sinter the LSCF. These cells are henceforth referred to as 'spray-pyrolyzed LSCF cell'.

The BCZY27 powder for the porous backbone was prepared by conventional solid state reaction of the same precursors as for the substrate, at 1400ºC for 30 h, followed by ball milling for 8 h. A slurry was prepared using the BCZY27 powder, Solsperse 20 wt% in Terpineol, dibutylphthalate as plasticizer and 5 wt% ethylcellulose in Terpineol as binder. The mixture was shaked for 24 h with zirconia balls. A layer was screen-printed on each side of the dense BCZY27 substrate with a Polyester 92 mesh with a speed of the blade of 60 $mm \cdot s^{-1}$. The samples were dried at 90°C in a rolling furnace and were then fired at 1300°C for 2 h (60°C·h^{-1} to 450°C and then 120°C·h^{-1}). The resulting BCZY27 porous backbone is beige/light brown. These cells are later on referred to as BCZY27|BCZY27|BCZY27.

Infiltration of the porous backbones was done by depositing a 3 mg drop on one side of the sample, followed by drying at 70°C on a heating plate. The same procedure was used on the second side. Between each infiltration, the samples were calcined at 350°C for 30 min. After the last infiltration, the calcination at 350°C was extended

to 2 h. The samples were infiltrated either 4 times or 12 times and were finally heated to 700°C for 2h (100°C h^{-1}). The infiltrated backbone became dark grey and black for the 4 times and 12 times infiltrated samples, respectively. These cells are later on referred to as '4LSCF cell' and' 12LSCF cell'.

2.3. Characterization

Crystallographic phases were determined by X-ray diffraction (XRD) at room temperature with a Bruker D8 Discover X-ray diffractometer in grazing incidence (θ=1°) for spray-pyrolyzed cells, and with a Stoe $\theta/2\theta$ X-ray diffractometer for the infiltrated cells.

The surface and cross-section morphologies of the cells were studied by field emission gun scanning electron microscopy (FEGSEM, FEI Quanta 200 or Zeiss Supra 35). Both unpolished and polished cross-sections were studied. All the micrographs presented are from secondary electron images. Deposition of a thin carbon layer was necessary because of the insulating properties of the samples. The porosity of the cathodes was determined from the polished cross section micrographs by determining the percentage of pores from the contrast of the micrographs on the basis of their intensity. The uncertainty of this determination is linked to the difficulty of fixing the intensity threshold. As a result, higher uncertainties are obtained for samples with nanoscale pores than in the case of samples with microscale pores.

For AC electrical measurements, gold current collectors (ESL Europe, type 8884G) were painted on the samples on the whole surface and heated to 700°C in air for 1 h (100°C·h^{-1}). After polishing of the edges, the samples were set in the testing rig, which allowed four samples to be tested at a time. Impedance spectra were recorded from 600°C to 450°C, with 50°C steps (cooling rate 1°C·min^{-1} and 2 h dwell before measurement) in three different steam conditions: (1) dry air directly from the compressed air line ($p(H_2O)$ < 0.001 atm), (2) air bubbled through a water bottle at 13°C ($p(H_2O)$ = 0.015 atm) and (3) air bubbled through a water bottle at 25°C ($p(H_2O)$ = 0.030 atm). The spectra were recorded with a Solartron 1260 impedance analyzer in the frequency range of 0.006 Hz to 1 MHz, with an amplitude of 100 mV. The spectra, after correction for the inductance of

the rig, were analyzed with *Zsimpwin* software using the circuits shown in the insert of Fig. 5 and 7. The area specific resistances were divided by two to take into account the geometry of the cells (two 'identical' cathodes). Two cells of each type were tested and the presented data are the average of these.

3. Results and discussion

The grazing incidence X-ray diffractogram of the spray-pyrolyzed LSCF cell demonstrates formation of single-phase LSCF after calcination at 700°C (see figure 1a). No secondary phases are observed, except the small peak at 2θ~29.5º which corresponds to the most intense peak (110) of the BCZY27 electrolyte.

Figure 1b shows the X-ray diffractrograms of a BCZY27|BCZY27|BCZY27 cell (no infiltration), a 4LSCF cell and a 12LSCF cell. One can note that the peaks of the BCZY27 phase (* symbol) are quite wide, due to the small size of the backbone crystallites, and a small lattice parameter difference between the dense BCZY27 prepared by solid state reactive sintering and the porous BCZY27 backbone prepared by conventional solid state reaction [31-32]. The peak intensity of the LSCF phase increases with the number of infiltrations, as expected.

The surface of the spray-pyrolyzed LSCF cell was covered with 1-2 µm thick ridges protruding from the substrate, with cauliflower-like structures in between (supporting doc 1). Such ridges typically form during spray pyrolysis when uneven substrate surfaces, long deposition times and low air pressure are used [33]. Because of the ridges, the thickness of the spray-pyrolyzed LSCF film is not homogeneous, but varies between 2 µm and 6 µm (figure 2a). The micrograph also reveals a good adhesion between the BCZY27 electrolyte and the LSCF layer. The porosity of the spray-pyrolyzed LSCF, determined from a high magnification micrograph (figure 2b), is (37±5)%. The relatively high uncertainty is due to the nanoscale size of the pores. In figure 2b it can be seen that a layered pore structure is formed as a result of the fabrication method and that the size of the individual pores is ~20 nm.

The grain size of the BCZY27 backbone after firing at 1300ºC for 2 h is between 200-500 nm. Some small cracks at the surface of the BCZY27 backbone are noticeable on the low magnification micrograph (supporting doc 2). The polished cross sections of the 4LSCF and 12LSCF cells are similar, with a thickness of 35-40 µm (figure 3). Micrographs with a magnification of 5000× (figure 3b) were used for the determination of the porosity for both the 4LSCF and the 12LSCF cells: (35±2)%. No difference in the porosity between the infiltrated cells and the non-infiltrated backbone could be noticed, nor was it possible to see the infiltrated LSCF from these polished cross sections. Non-polished cross sections of the 4LSCF and 12LSCF cells are shown in figure 4. The brighter areas (50 nm) correspond to the LSCF, which was found to be present in the full thickness of the cathode. However, one can note that the infiltrated LSCF doesn't form a network (no percolation), meaning that only the LSCF in contact with the current collector (i.e. at the surface) functions as cathode material during the electrochemical characterization. The mass loading of LSCF was estimated to 2-2.5% and ~7% (compared to the mass of the porous BCZY27 backbone) for 4LSCF and 12LSCF respectively.

Figure 5a presents the spectra recorded on the spray-pyrolyzed LSCF cell with gold current collectors at 550ºC in air with different water vapour pressures. All the spectra were fitted with the equivalent circuit $(R_1Q_1)(R_2Q_2)(R_3Q_3)(R_4Q_4)$. If the two middle (RQ) circuits were replaced by a Gerischer element (G) or a finite length Warburg element (O) the quality of fit decreased. The different impedance arcs were allocated to the corresponding processes using the pseudo capacitance (C) related to each arc. As a result, R_1 corresponds to the electrolyte (C_1~$4\cdot10^{-11}$ F·cm^{-2}) and R_2, R_3 and R_4 to the cathode (C_2~$6\cdot10^{-6}$ F·cm^{-2}, C_3~$2\cdot10^{-5}$ F·cm^{-2} and C_4~$6\cdot10^{-2}$ F·cm^{-2}). An example of fit for the spectrum recorded at 550ºC in air with $p(H_2O)$=0.03 atm is shown in figure 5b. According to Dailly *et al.* [12], semicircles with pseudo capacitance in the range $4\cdot10^{-3}$-10^{-5} F·cm^{-2} can be assigned to the charge transfer reaction (transfer of the protons from the electrolyte to the electrode) and the lower frequency semi circle ($C=3\cdot10^{-3}$-10^{-2} F·cm^{-2}) to the electrode reaction process (oxygen dissociation/ adsorption steps overlapping with the diffusion process). By analogy, (R_4Q_4) can be appointed to the oxygen dissociation/adsorption due to the high capacitance. (R_2Q_2) and (R_3Q_3), due to their capacitance values, can be assigned to charge transfer. One can also note from figure 5a that the resistance of the electrolyte decreases with

increasing water vapour pressure, as expected for a proton conductor, while the polarization resistance (cathode contribution) increases. The area specific resistances for the charge transfer (sum of R_2 and R_3) and for the oxygen dissociation/adsorption (R_4) are shown as a function of the inverse temperature in figures 6a and 6b, respectively. Both area specific resistances are thermally activated. The increase of the polarization resistance with increasing water vapour pressure was not anticipated, as it does not correspond to any of the eight steps proposed by He *et al.* [34] for the cathode mechanism, rather it was expected that the polarization resistance would decrease with increasing water vapour pressure due to increased proton incorporation into the electrolyte. However, this phenomenon was also observed for LSCF cathodes by Grimaud [35]. Long-term degradation studies of LSCF at 700-750 °C in presence of water vapour have demonstrated Sr enrichment at the surface [36-37], which could decrease the oxygen exchange due to strontium hydroxide formation. But we do not believe Sr enrichment is the cause of the increased resistance. Firstly, compared to the long-term degradation experiments [36, 37] the temperature was lower and the time shorter in our impedance measurements. Secondly, no degradation of the cathode material was observed over the testing period (about 3 weeks). A final spectrum was recorded with temperature and atmosphere conditions similar to those of the first spectrum and no changes were observed. Thirdly, the A-site deficiency of LSCF ($La_{0.58}Sr_{0.4}Co_{0.2}Fe_{0.8}O_{3-\delta}$) was chosen to limit/avoid Sr enrichment at the surface [38] with possible hydroxide or carbonate formation in wet or CO_2-containing atmosphere, respectively. Grimaud [35] compared the performances of several cathode materials: LSCF, $Ba_{0.5}Sr_{0.5}Co_{0.8}Fe_{0.2}O_{3-\delta}$ (BSCF), $Pr_2NiO_{4+\delta}$ and $PrBaCo_2O_{5+\delta}$. He observed that LSCF was the only material which did not exhibit proton conduction and whose polarization resistance increased with increasing water vapour pressure. For the other compounds, which showed proton conduction (even though rather limited), the polarization resistance decreased with increasing water vapour pressure (in agreement with the steps proposed by He *et al.* [34]). Thus, the main difference between LSCF and the other cathode materials is the localization of the active sites for the cathode reaction: they are limited to the to the triple phase boundaries (TPB) at the interface cathode/electrolyte in the case of LSCF, whereas all the surface of the cathode material is active (in addition to

the TPBs at the interface cathode/electrolyte) in the case of BSCF, $Pr_2NiO_{4+\delta}$ and $PrBaCo_2O_{5+\delta}$. As a result, we can conclude that the increase of the polarization resistance with increasing water vapour pressure for LSCF has its origin at the TPBs. However, to be able to understand what really takes place at the TPBs, additional experiments such as cone electrode measurements [39-40] will have to be done.

The spectra of the infiltrated 4LSCF and 12LSCF cells were fitted with the equivalent circuit $(R_aQ_a)(R_bQ_b)(R_cQ_c)$. As previously, the different semi-circles were attributed to the corresponding processes using the pseudo capacitance related to each constant phase element. R_a corresponds to the BCZY27 electrolyte/backbone (C_a~$4\cdot10^{-11}$ F·cm^{-2}), R_b (C_b~$1.6\cdot10^{-6}$ F·cm^{-2}) to the charge transfer and R_c to the oxygen dissociation/adsorption (C_c~$3.2\cdot10^{-2}$ F·cm^{-2}). An example is shown in figure 7 in the case of 12LSCF at 550 ºC in air with $p(H_2O)$=0.03 atm. Only one (RQ) circuit was necessary for fitting the charge transfer contribution, in comparison to two, in the case of the spray-pyrolyzed LSCF cells.

The total conductivity of the BCZY27 electrolyte/backbone (calculated from R_a) is plotted in figure 8a in the case of 12LSCF, with similar results obtained for 4LSCF. There is a clear increase of the conductivity of BCZY27 with increasing water vapour pressure, as expected for a proton conductor based on hydration. Furthermore, these conductivity values for BCZY27 electrolyte/backbone are lower than those of the spray-pyrolyzed cell, due to the difference of the cell geometry: the presence of a porous backbone reduces significantly the total conductivity of the BCZY27. This can be attributed to the increased dominance of grain boundaries in the backbone, as the grain boundary conduction is much lower than the bulk conduction in these materials [41]. The area specific resistances for the charge transfer and the oxygen dissociation/adsorption of the 12LSCF and 4LSCF cells are shown in figure 8b and c. Both of these area specific resistances increase with increasing water vapour pressure as for the spray-pyrolyzed LSCF cell. As expected, they are lower for the 12LSFC cell than for the 4LSCF cell due to the larger amount of cathode material and, therefore, larger area where the water vapour can be formed. As shown in figure 4, and mentioned above, the infiltrated LSCF does

not percolate (for both 4LSCF and 12LSCF), meaning that only the LSCF in contact with the current collector is active.

Table 1 summarizes the area specific resistances of the cathode for the three kinds of symmetric cell (spray-pyrolyzed LSCF cell, 4LSCF, 12LSCF) at 500ºC and 600ºC in air, at different water vapour pressures. In the case of the spray-pyrolyzed LSCF, the area specific resistance corresponds to the sum of R_2, R_3 and R_4 while for the infiltrated cells it corresponds to the sum of R_b and R_c.

By using the same cathode material (LSCF) but changing the geometry of the cell by using different fabrication methods (spray pyrolysis or infiltration into a porous backbone), the importance of the area where protons/oxygen/electrons are present to form water can be highlighted. This area, being higher for 12LSCF compared to the one of 4LSCF due to more cathode material, results in a lower area specific resistance. The performance difference between the spray-pyrolyzed LSCF cell and the 12LSCF cell is small, especially at 600 °C (table 1). However, the different microstructure of the two cells has a clear influence when the area specific resistance is divided into charge transfer and oxygen dissociation/adsorption contributions (figures 6 and 8). The charge transfer resistance is lowest for the 12LSCF cell, due to the high number of triple phase boundaries between the BZCY27 backbone and infiltrated LSCF. But the resistance attributed to oxygen dissociation/adsorption processes is lowest for the spray-pyrolyzed LSCF cell, probably due to the larger total surface area available for oxygen molecules to adsorb and split into oxygen ions, and maybe also due to better contact with the current collector so that a larger part of the cathode can be active. Thus, the importance of maximizing both triple phase boundaries and active cathode surface area is demonstrated.

The cathode area specific resistance values (R_p), at 600ºC in air, obtained in this work are compared to literature values obtained with symmetric cells in table 2. Our R_p values are clearly among the lowest reported and are a decade lower than previously reported for $La_{0.6}Sr_{0.4}Co_{0.2}Fe_{0.8}O_{3-\delta}$. Compared to the $La_{0.6}Sr_{0.4}Co_{0.2}Fe_{0.8}O_{3-\delta}$ cathodes studied by Dailly et *al*. [12], the lower R_p values are mainly due to a lower contribution for the oxygen

dissociation/adsorption. But also the A-site deficiency in our LSCF cathodes can be of importance as there are more oxygen vacancies which increase the oxygen ion diffusion. As all the other cathodes in table 2 were made by powder methods, the low-temperature fabrication methods described here are very promising for obtaining high-performance cathodes for proton-conducting electrolytes.

In addition to the measurements cited in table 2 several groups have studied cathode performance using single cells (anode|electrolyte|cathode) [7,11,14-17,20-21]. But as a result of the single cell geometry, the measured polarization resistance corresponds to the combined contribution of the anode and the cathode and cannot therefore be compared to the data of this work.

The activation energy values for the polarization resistances were calculated from the Arrhenius plots for the two cathode contributions and are listed in table 3, for the spray-pyrolyzed LSCF and 12LSCF. Most of the papers in the literature provide the activation energy value related to the total polarization resistance of the cathode [26,42]. However, we prefer to split it for each semi-circle as it gives a better insight of the processes. The activation energy for the low frequency contribution (oxygen dissociation/adsorption) is in the same range for both compounds: between 1.01 and 1.21 eV, which is sensible as the oxygen dissociation/adsorption takes place on the LSCF and is therefore independent on the sample geometry. A similar value was reported by He *et al.* [34] (1.17 eV) in the case of composite cathode ($Sm_{0.5}Sr_{0.5}CoO_{3-d}$ (SSC)–$BaCe_{0.8}Sm_{0.2}O_{3-d}$ (BCS)) and was assigned to the surface dissociative adsorption and diffusion of oxygen. One can also see that the activation energy of this contribution increases with the water vapour pressure. In contrast, the activation energy for the middle range frequency contribution (charge transfer) depends on the geometry of the sample. The value for the 12LSCF (0.56-0.76 eV) is close to that of proton conduction [31, 34, 43] whereas the value of ~1.2 eV for the spray-pyrolyzed LSCF is similar to that of the oxygen dissociation/adsorption contribution. He *et al*. [34] and Wu *et al.* [44] reported activation energy values for the charge transfer of ~0.60 eV and between 0.65 eV and 0.75 eV, respectively, corresponding to the transfer of protons from the electrolyte to the triple phase boundaries. This is in agreement with the value for 12LSCF. The higher value determined in this study for the spray-

pyrolyzed LSCF is characteristic of oxygen transfer [34]. Even though it is not possible to explain fully the mechanism of the cathode processes from this set of data, we can underline the difference of charge transfer between a mixed oxide ion and electron conducting cathode when it is deposited on a proton-conducting electrolyte (spray-pyrolyzed LSCF) and when it is infiltrated into a proton-conducting electrolyte (12LSCF).

While the LSCF cathodes reported here are promising, there is still room for improvement. The results show that both a high amount of triple phase boundaries and a large cathode surface area reduce the cathode area specific resistance. The decrease of the resistance by a factor of 7 between the 4LSCF cell and the 12LSCF cell is encouraging. If the infiltrated LSCF can be made to percolate through the whole thickness of the porous backbone, a much better cathode performance can be obtained. A better percolation could be achieved by increasing the concentration of the solution used for the infiltration or by increasing the number of infiltrations. For spray-pyrolyzed cells, deposition onto a rougher electrolyte surface (non-polished) could increase the contact area between electrolyte and cathode and thereby reduce the charge transfer resistance. The solution routes that are described here can be used for a variety of cathode materials simply by changing the precursors in the solution. These routes are also promising for metal-supported fuel cells which require much lower processing temperatures than traditional ceramic-supported SOFCs/PCFCs.

4. Conclusions

Two solution routes for fabrication of LSCF cathodes for PCFC were compared: spray pyrolysis and infiltration. Symmetric cells (cathode|electrolyte|cathode) based on a proton-conducting oxide (BCZY27) were prepared with spray-pyrolyzed LSCF or with infiltrated LSCF in a porous BZCY27 backbone, the latter being screen printed on the dense electrolyte. Calcination for 2 h at 700°C was sufficient for LSCF formation. The spray-pyrolyzed LSCF cathode was between 2 and 6 µm thick with presence of ridges. Much thicker cathodes (35-40 µm) were obtained with the infiltration of LSCF in the BCZY27 porous backbone. However, as the infiltrated LSCF did not percolate through the thickness of the porous backbone, only the LSCF in contact with the current

collector acted as cathode. Impedance spectra were recorded on the symmetric cells between 450°C and 600°C in air with different water vapour pressures and showed two contributions for the cathode: charge transfer and dissociation/adsorption of oxygen. For all the cells, the cathode resistances were found to increase with increasing water vapour pressure. Area specific resistances of 0.61 $\Omega \cdot cm^2$ and 0.89 $\Omega \cdot cm^2$ were obtained at 600°C for the spray-pyrolyzed LSCF cell in dry air and in air with $p(H_2O)$=0.03 atm, respectively. Slightly higher values (0.63 $\Omega \cdot cm^2$ and 0.98 $\Omega \cdot cm^2$ in dry air and in air with $p(H_2O)$=0.03 atm, respectively) were obtained for the porous backbone infiltrated 12 times with LSCF (which are much lower than that obtained on a cell infiltrated only 4 times with LSCF (4.3 $\Omega \cdot cm^2$ and 6.5 $\Omega \cdot cm^2$)). The obtained values are among the lowest reported for cathodes for PCFC, especially for LSCF cathodes. The activation energies calculated for the polarization resistance of both cathode contributions revealed an interesting feature: whereas similar values were obtained for the dissociation/adsorption of oxygen for the spray-pyrolyzed LSCF and 12LSCF (1.01-1.21 eV) there is a difference for the charge transfer contribution: with an activation energy characteristic of proton conduction for 12LSCF (0.56-0-76 eV) and of oxide ion conduction for spray-pyrolyzed LSCF (about 1.2 eV). To determine the rate limiting step for each contribution of the cathode polarization resistance, both oxygen and water vapour dependences are needed [34,43].

Spray pyrolysis and infiltration are promising fabrication methods for PCFC cathodes; the lower processing temperature maintains the small size of cathode and backbone particles which are essential for having a large amount of triple phase boundaries and a high surface area.

Acknowledgments

This work was carried out within the nextgenFCmat project (*Next generation fuel cell materials)*, financed by The Danish Council for Strategic Research (DSF case number 09-075900) and by The Research Council of Norway (#197935). The authors would also like to thank Martin Søgaard from Risø DTU for useful discussions.

References

1. K.D. Kreuer, Annu. Rev. Mater. Res. 33 (2003) 333-359

2. L. Malavasi, C.A.J. Fischer, M.S. Islam, Chem. Soc. Rev. 39 (2010) 4370-4387

3. E. Fabbri, D. Pergolesi, E. Traversa, Chem. Soc. Rev. 39 (2010) 4366-4369

4. R. Peng, Y. Wu, L. Yang, Z. Mao, Solid State Ionics 177 (2006) 389-393

5. Y. Lin, R. Ran, Y. Zheng, Z. Shao, W. Jin, N. Xu, J. Ahn, J. Power Sources 180 (2008) 15-22

6. J. Dailly, S. Fourcade, A. Largeteau, F. Mauvy, J.C. Grenier, M. Marrony, Electrochim. Acta 55 (2010) 5847-5853

7. L. Yang, Z. Liu, S. Wang, Y. Choi, C. Zuo, M. Liu, J. Power Sources 195 (2010) 471-474

8. E. Fabbri, S. Licoccia, E. Traversa, E.D. Wachsman, Fuel Cells 2 (2009) 128–138

9. Q. Ma, R. Peng, Y. Lin, J. Gao, G. Meng, J. Power Sources 161 (2006) 95-98

10. T. Hibino, A. Hashimoto, M. Suzuki, M. Sano, J. Electrochem. Soc. 149 (2002) A1503-A1508

11. H. Ding, B. Lin, Y. Jiang, S. Wang, D. Fang, Y. Dong, S. Tao, R. Peng, X. Liu, G. Meng, J. Power Sources 185 (2008) 937-940

12. J. Dailly, F. Mauvy, M. Marrony, M. Pouchard, J.C. Grenier, J. Solid State Electrochem. 15 (2011) 245-251

13. V.B. Vert, C. Solís, J.M. Serra, Fuel Cells 1 (2011) 81–90

14. L. Zhao, B. He, Y. Ling, Z. Xun, R. Peng, G. Meng, X. Liu, Int. J. Hydrogen Energy 35 (2010) 3769-3774

15. Z. Tao, L. Bi, Z. Zhu, W. Liu, J. Power Sources 194 (2009) 801-804

16. W. Sun, Z. Zhu, Y. Jiang, Z. Shi, L. Yan, W. Liu, Int. J. Hydrogen Energy (2011) doi:10.1016/j.ijhydene.2011.04.222

17. L. Zhao, B. He, B. Lin, H. Ding, S. Wang, Y. Ling, R. Peng, G. Meng, X. Liu, J. Power Sources 194 (2009) 835-837

18. Q. Nian, L. Zhao, B. He, B. Lin, R. Peng, G. Meng, X. Liu, J. Alloy Compd 492 (2010) 291-294

19. L. Yang, C. Zuo, S. Wang, Z. Cheng, M. Liu, Adv. Mater. 20 (17) (2008) 3280-3283

20. B. Lin, H. Ding, Y. Dong, S. Wang, X. Zhang, D. Fang, G. Meng, J. Power Sources 186 (2009) 58-61

21. Y. Lin, R. Ran, C. Zhang, R. Cai, Z. Shao, J. Phys. Chem. A 114 (2010) 3764–3772

22. H.B. Yahia, F. Mauvy, J.C. Grenier, J. Solid State Chem. 183 (2010) 527–531

23. M. Shah, S.A. Barnett, Solid State Ionics 179 (2008) 2059-2064

24. M.F. Han, Z. Liu, J. Qian, ECS Transaction 35 (2011) 2295-2303

25. J. Chen, F. Liang, L. Liu, S. Jiang, B. Chi, J. Pu, J. Li, J. Power Sources 183 (2008) 586-589

26. X. Lou, Z. Liu, S. Wang, Y. Xiu, C.P. Wong, M. Liu, J. Power Sources 195 (2010) 419-424

27. M.B. Larsen, M. Sc. thesis, Optimization of infiltration solutions for improving performance of SOC electrodes, Risø DTU, June 2010

28. D. Perednis, L.J. Gauckler, J. Electroceram. 14 (2005) 103-111

29. D. Beckel, U.P. Muecke, T. Gyger, G. Florey, A. Infortuna, L.J. Gauckler, Solid State Ionics 178 (2007) 407-415

30. D. Marinha, J. Hayd, L. Dessemond, E. Ivers-Tiffée, E. Djurado, J. Power Sources 196 (2011) 5084-5090

31. S. Ricote, N. Bonanos, Solid State Ionics 181 (2010) 694-700

32. S. Ricote, N. Bonanos, A. Manerbino, W.G. Coors, J. Hydrogen Energy (2011) doi:10.1016/j.ijhydene.2011.08.118

33. D. Beckel, A. Dubach, A.R. Studart, L.J. Gauckler, J. Electroceram. 16 (2006) 221-228

34. F. He, T. Wu, R. Peng, C. Xia, J. Power Sources 194 (2009) 263-268

35. A. Grimaud, PhD thesis, Propriété de conduction mixte $O^{2-}/H^{+}/e^{-}$ dans quelques phases derivées de la pérovskite: application aux cathodes de piles à combustible H+-SOFC, Université de Bordeaux, ICMCB-CNRS, 2011.

36. E. Bucher, W. Sitte. Solid State Ionics 192 (2011) 480–482

37. S. Simner, M. Anderson, M. Engelhard, J. Stevenson. Electrochem Solid State Letters 9 (2006) A478-A481

38. A. Mai, V.A.C. Haanappel, S. Uhlenbruck, F. Tietz, D. Stöver, Solid State Ionics 176 (2005) 1341-1350

39. M. Odgaard, E. Skou, Solid State Ionics 86–88 (1996) 1217–1222

40. P. Fabry, M. Kleitz, Journal of Electroanalytical Chemistry and Interfacial Electrochemistry, 57 (1974) 165–177

41. S. Ricote, N. Bonanos, G. Caboche, Solid State Ionics 180 (2009) 990-997

42. H. Zhao, F. Mauvy, C. Lalanne, J.-M. Bassat, S. Fourcade, J.-C. Grenier, Solid State Ionics 179 (2008) 2000-2005

43. R. Peng, T. Wu, W. Liu, X. Liu, G. Meng, J. Mater. Chem. 20 (2010) 6218-6225

44. T. Wu, Y. Zhao, R.Peng, C. Xia, Electrochim. Acta 54 (2009) 4888-4892

Table(s)

Table 1: Cathode area specific resistances (in $\Omega \cdot cm^2$) for the three types of symmetric cells in air.

	Spray-pyrolyzed LSCF			**4LSCF**			**12LSCF**		
	Dry	$p(H_2O)$= 0.015 atm	$p(H_2O)$= 0.03 atm	Dry	$p(H_2O)$= 0.015 atm	$p(H_2O)$= 0.03 atm	Dry	$p(H_2O)$= 0.015 atm	$p(H_2O)$= 0.03 atm
500ºC	6.52	6.68	10.8	36	52.4	55.7	4.6	5.4	6.1
600ºC	0.61	0.77	0.89	4.3	6.2	6.5	0.63	0.86	0.98

Table 2: Comparison of cathode area specific resistances obtained with symmetric cells (cathode|electrolyte|cathode) containing proton-conducting electrolyte, in air at 600ºC.

Cathode compound	Electrolyte	Cathode fabrication method	R_p ($\Omega \cdot cm^2$)	Ref.
$Ba_{0.5}Sr_{0.5}Co_{0.8}Fe_{0.2}O_{3-\delta}$	$BaCe_{0.9}Y_{0.1}O_{3-\delta}$	Screen printing	~1.5	[12]
		Spray-deposition of slurry	~0.5	[5]
$La_{0.6}Sr_{0.4}Co_{0.2}Fe_{0.8}O_{3-\delta}$	$BaCe_{0.9}Y_{0.1}O_{3-\delta}$	Screen printing	~6	[12]
	$BaCe_{0.9}Y_{0.1}O_{3-\delta}$	Painting of slurry	~7.9	[8]
$La_{0.58}Sr_{0.4}Co_{0.2}Fe_{0.8}O_{3-\delta}$ (LSCF)	BZCY27	Spray pyrolysis	0.61	This work
		Infiltration into porous backbone	0.63	This work
Pr_2NiO_{4+d}	$BaCe_{0.9}Y_{0.1}O_{3-\delta}$	Screen printing	~1.5	[12]
$PrBaCo_2O_{5+\delta}$	$BaZr_{0.1}Ce_{0.7}Y_{0.2}O_{3-\delta}$	Spray deposition of slurry	0.73	[21]
$Y_{0.5}Pr_{0.5}BaCo_2O_{5+\delta}$	$BaZr_{0.1}Ce_{0.7}Y_{0.2}O_{3-\delta}$	Spray deposition of slurry	0.59	[21]
$Ca_3Co_4O_{9+\delta}$	$BaCe_{0.9}Y_{0.1}O_{3-\delta}$	Painting of slurry	2.2	[22]
$La_{0.6}Sr_{0.4}Co_{0.2}Fe_{0.8}O_{3-\delta}$/$BaCe_{0.9}Yb_{0.1}O_{3-\delta}$ composite (1:1 by weight)	$BaCe_{0.8}Y_{0.2}O_{3-\delta}$	Painting of slurry	~1.1	[8]
$Pr_{0.58}Sr_{0.4}Fe_{0.8}Co_{0.2}O_{3-\delta}$/$BaCe_{0.9}Yb_{0.1}O_{3-\delta}$ composite (60:40 by volume)	$BaCe_{0.9}Y_{0.1}O_{3-\delta}$	Screen printing	~1.2	[13]

Table 3: Activation energy (eV) of the cathode polarization. R_{ct} and R_{ox} correspond to the polarization resistance of the charge transfer and of the oxygen dissociation/adsorption respectively.

	Spray-pyrolyzed LSCF			**12LSCF**		
	Dry	$p(H_2O)$= 0.015 atm	$p(H_2O)$= 0.03 atm	Dry	$p(H_2O)$= 0.015 atm	$p(H_2O)$= 0.03 atm
Ea R_{ct}	1.2	1.2	1.21	0.76	0.62	0.56
Ea R_{ox}	1.06	1.19	1.21	1.01	1.06	1.21

Figure caption

Figure 1: (a) Grazing incidence X-ray diffractogram of the spray-pyrolyzed LSCF cell, (b) X-ray diffractograms of the BCZY27|BCZY27|BCZY27 cell, the 4LSCF cell, and the 12LSCF cell.

Figure 2: FEGSEM micrographs of a polished cross section of a spray-pyrolyzed LSCF cell: (a) dense BCZY27 electrolyte with spray-pyrolyzed LSCF on top and (b) spray-pyrolyzed LSCF layer.

Figure 3: FEGSEM micrographs of a polished cross section of 12LSCF: (a) dense BCZY27 electrolyte with porous BCZY27 backbone infiltrated with LSCF, and (b) BCZY27 backbone infiltrated with LSCF.

Figure 4: FEGSEM micrographs of non-polished cross sections of (a) a 4LSCF cell, and (b) a 12LSCF cell.

Figure 5: (a) AC spectra of the spray-pyrolyzed LSCF cell at 550ºC in air with different water vapour pressures, (b) fit of the AC spectrum recorded on the spray-pyrolyzed LSCF cell at 550ºC in air with $p(H_2O)$=0.03 atm. The solid lines correspond to the fit and the dots to the experimental data. The equivalent circuit used for fitting is shown in (b).

Figure 6: Area specific resistances (ASR) corresponding to the cathode processes for the spray-pyrolyzed LSCF cell in air with different water vapour pressures: (a) charge transfer (b) oxygen dissociation/adsorption.

Figure 7: AC spectrum recorded of the 12LSCF cell at 550ºC in air with $p(H_2O)$=0.03 atm. The solid lines correspond to the fit using the shown equivalent circuit, and the dots to the experimental data.

Figure 8: (a) Conductivity of the BCZY27 electrolyte/backbone for the 12LSCF cell in air with different water vapour pressures. And area specific resistances for (b) the charge transfer and (c) the oxygen dissociation/adsorption.

Figure 1

Click here to download Figure(s): Fig 1.doc

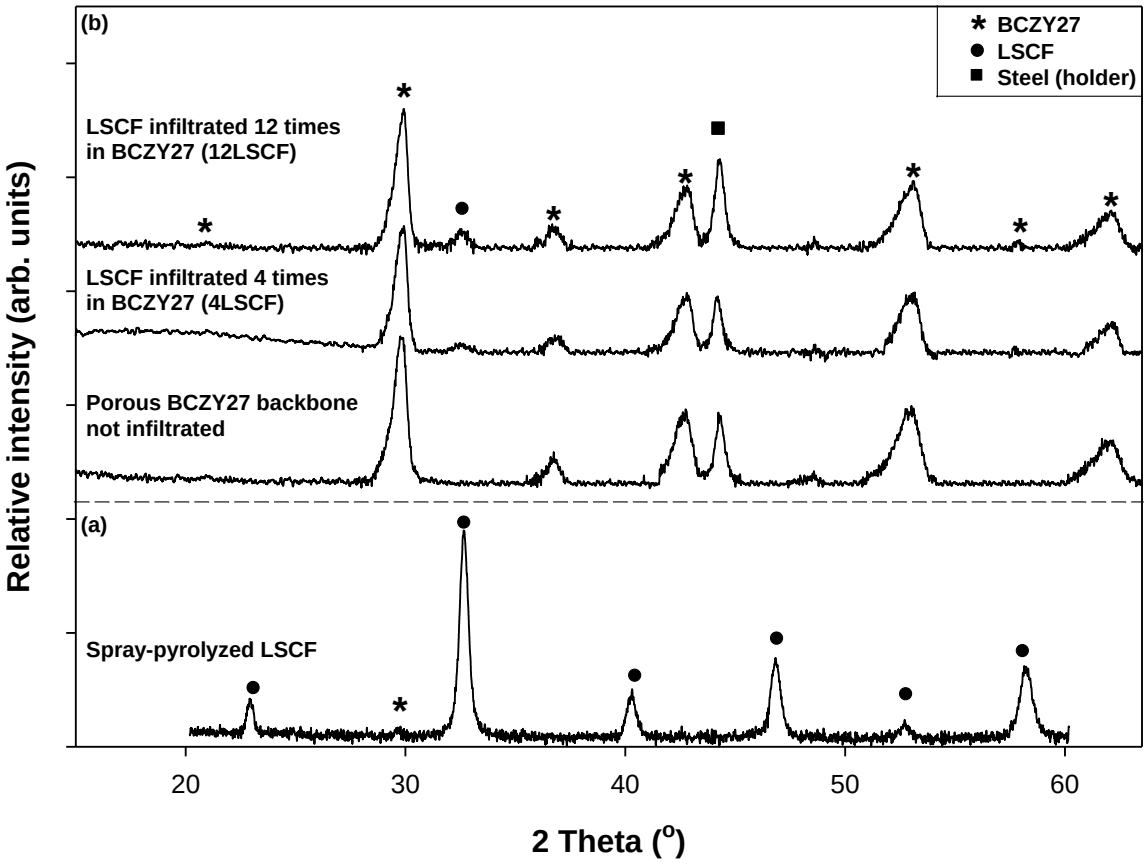

Figure 2

Click here to download high resolution image

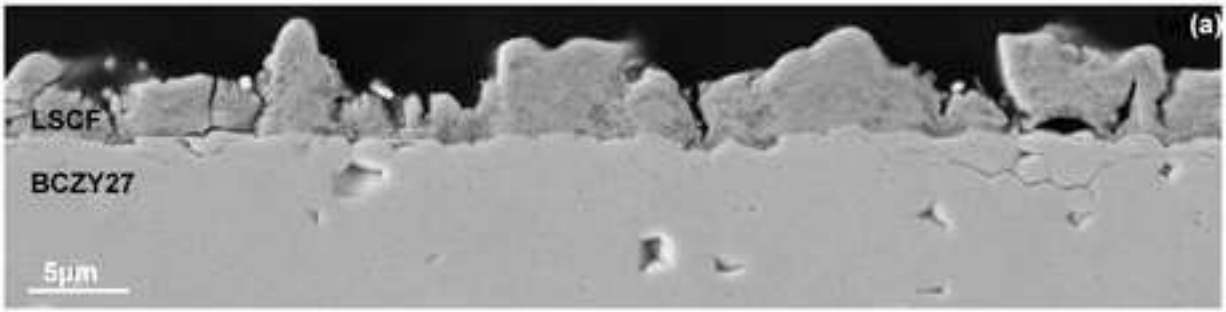

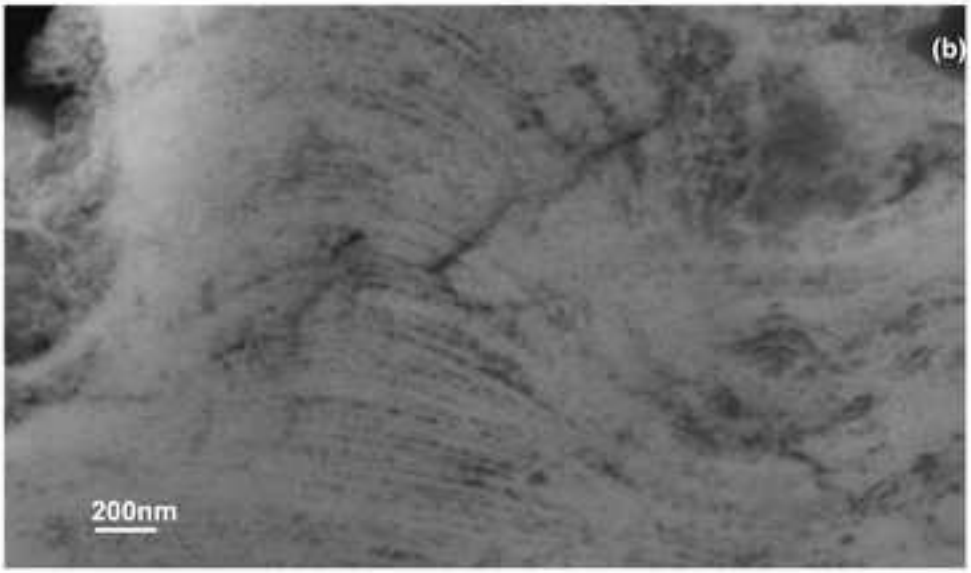

Figure 3

Click here to download high resolution image

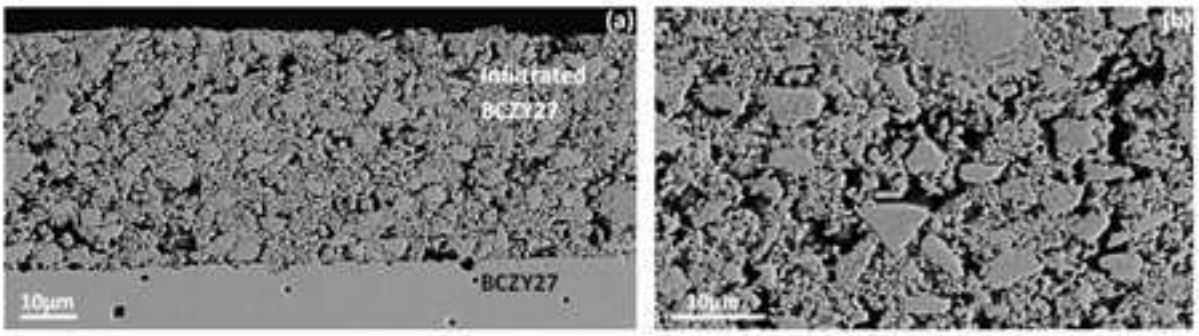

Figure 4

Click here to download Figure(s): fig 4 more contrast.doc

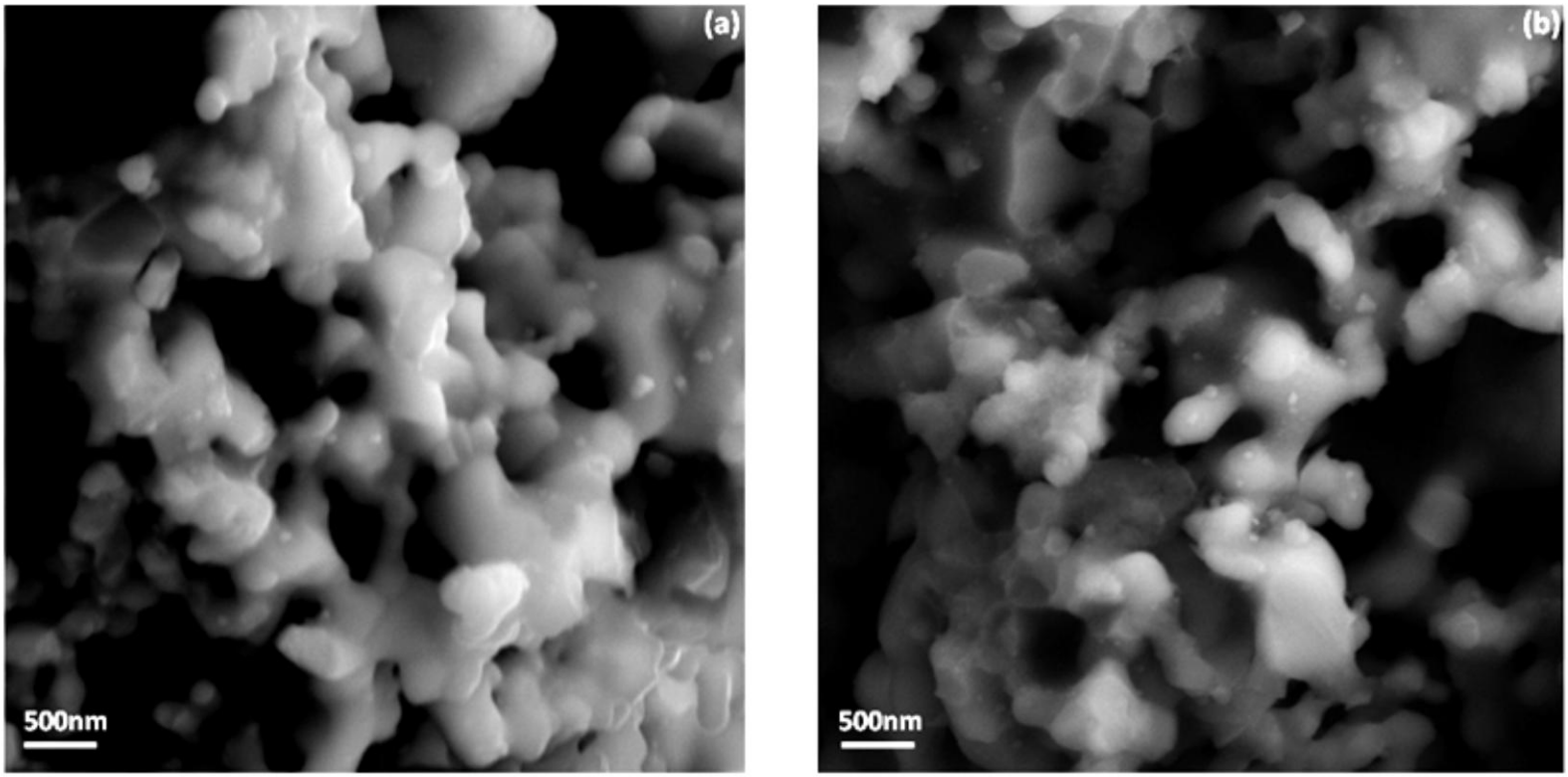

Figure 5

Click here to download Figure(s): fig 5.doc

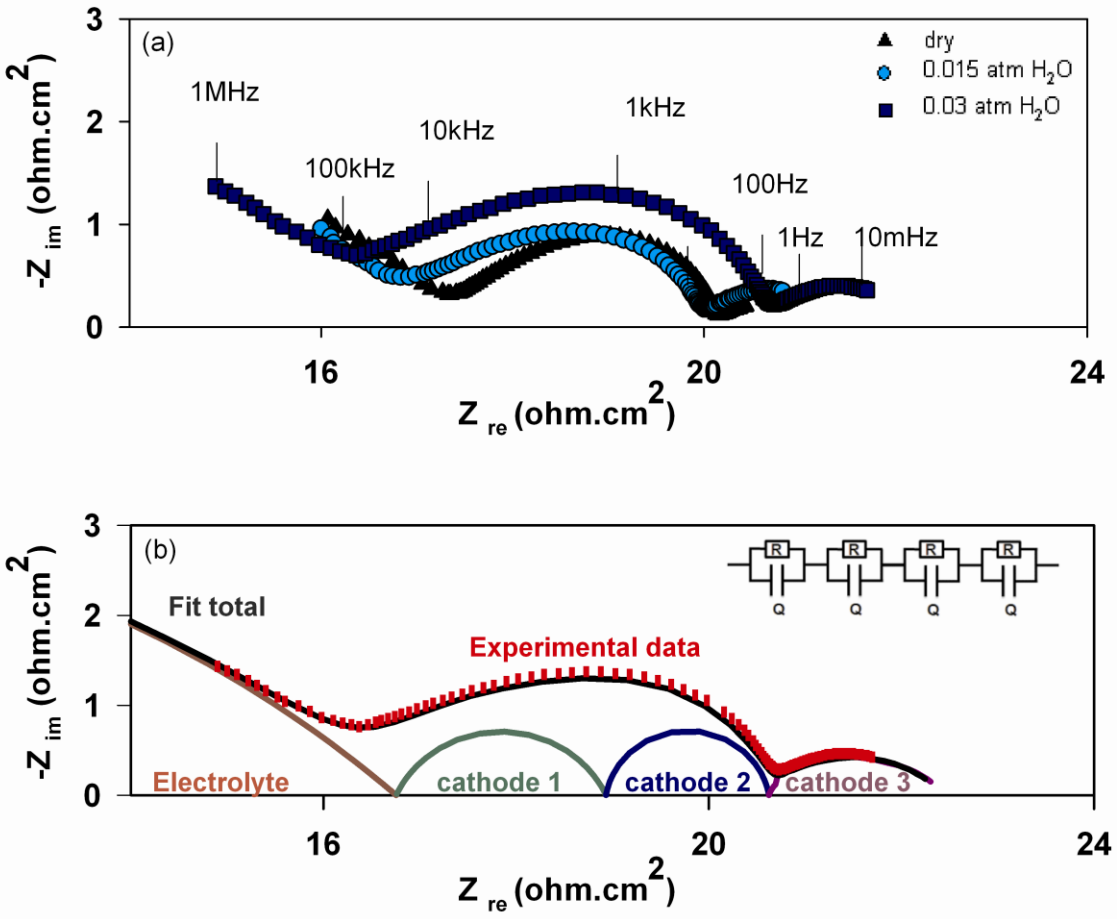

Figure 6

Click here to download Figure(s): fig 6.doc

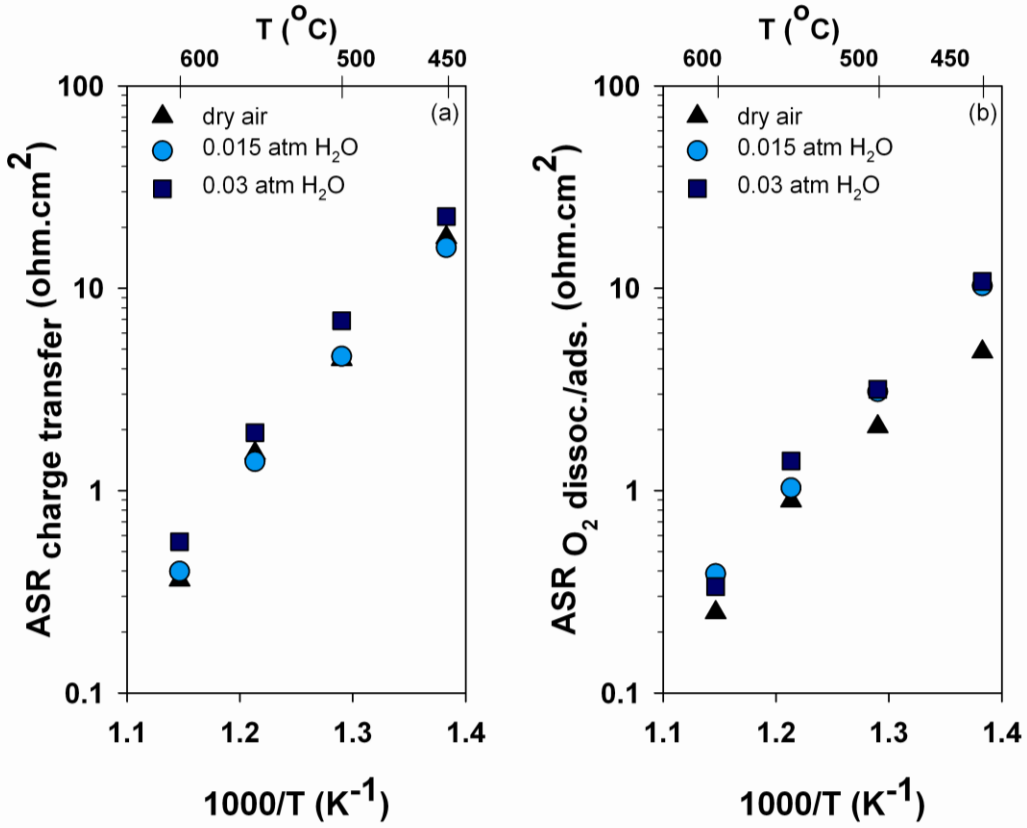

Figure 7

Click here to download Figure(s): fig 7.doc

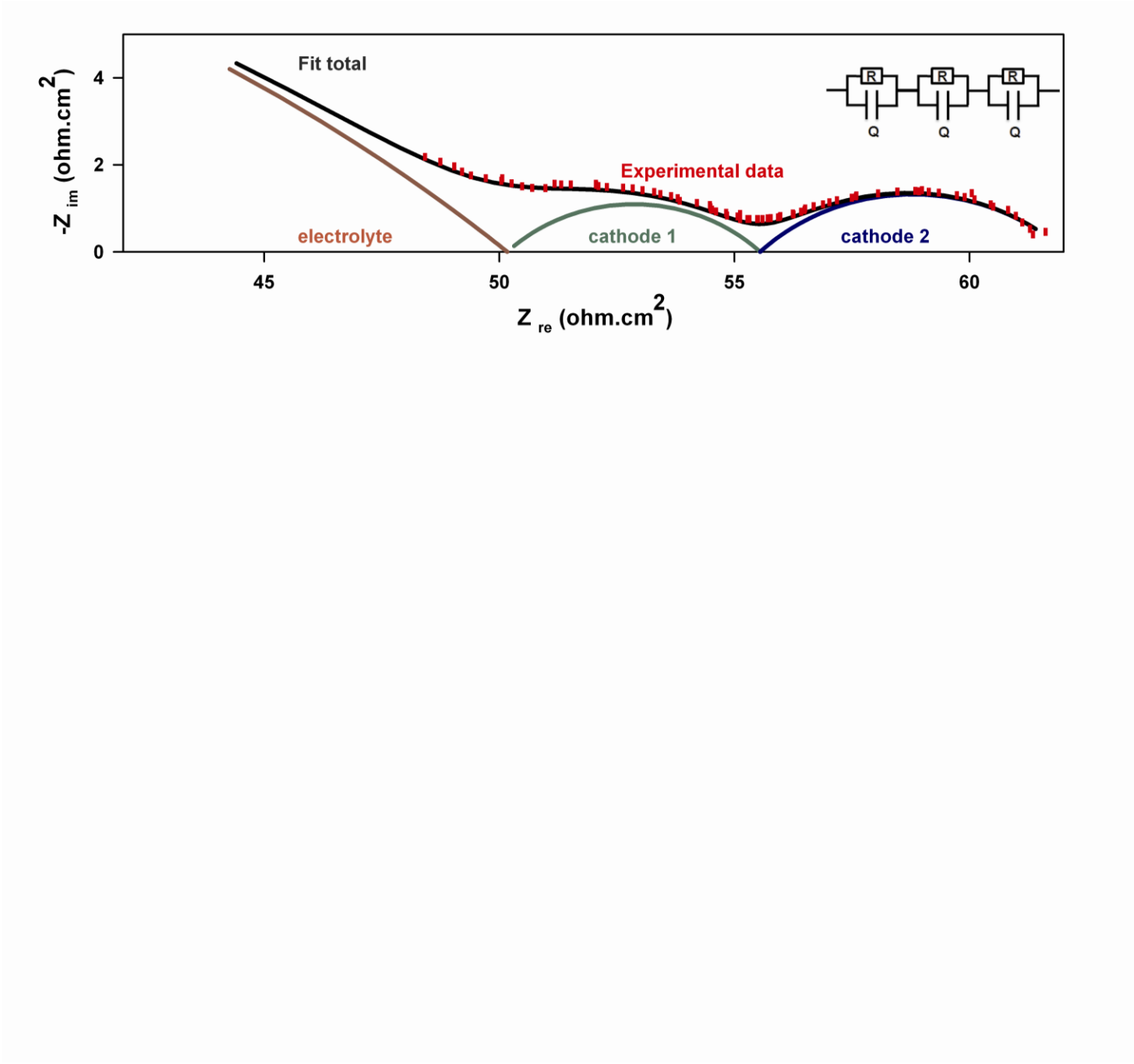

Figure 8

Click here to download Figure(s): fig 8.doc